

Amplitude inversion of the 2D analytic signal of magnetic anomalies through the differential evolution algorithm^{*}

Yunus Levent Ekinci^{1,2} , Şenol Özyalın³, Petek Sındırgı³,
Çağlayan Balkaya⁴  and Gökhan Göktürkler³ 

¹ Bitlis Eren University, Department of Archaeology, Bitlis, Turkey

² Bitlis Eren University, Career Research and Application Center, Bitlis, Turkey

³ Dokuz Eylül University, Department of Geophysical Engineering, İzmir, Turkey

⁴ Süleyman Demirel University, Department of Geophysical Engineering, Isparta, Turkey

E-mail: ylekinci@beu.edu.tr

Received 25 April 2017

Accepted for publication 17 July 2017

Published 8 November 2017



CrossMark

Abstract

In this work, analytic signal amplitude (ASA) inversion of total field magnetic anomalies has been achieved by differential evolution (DE) which is a population-based evolutionary metaheuristic algorithm. Using an elitist strategy, the applicability and effectiveness of the proposed inversion algorithm have been evaluated through the anomalies due to both hypothetical model bodies and real isolated geological structures. Some parameter tuning studies relying mainly on choosing the optimum control parameters of the algorithm have also been performed to enhance the performance of the proposed metaheuristic. Since ASAs of magnetic anomalies are independent of both ambient field direction and the direction of magnetization of the causative sources in a two-dimensional (2D) case, inversions of synthetic noise-free and noisy single model anomalies have produced satisfactory solutions showing the practical applicability of the algorithm. Moreover, hypothetical studies using multiple model bodies have clearly showed that the DE algorithm is able to cope with complicated anomalies and some interferences from neighbouring sources. The proposed algorithm has then been used to invert small- (120 m) and large-scale (40 km) magnetic profile anomalies of an iron deposit (Kesikköprü-Bala, Turkey) and a deep-seated magnetized structure (Sea of Marmara, Turkey), respectively to determine depths, geometries and exact origins of the source bodies. Inversion studies have yielded geologically reasonable solutions which are also in good accordance with the results of normalized full gradient and Euler deconvolution techniques. Thus, we propose the use of DE not only for the amplitude inversion of 2D analytical signals of magnetic profile anomalies having induced or remanent magnetization effects but also the low-dimensional data inversions in geophysics.

Keywords: magnetic anomalies, 2D analytic signal amplitude, optimization, differential evolution, parameter tuning, normalized full gradient, Euler deconvolution

(Some figures may appear in colour only in the online journal)

1. Introduction

One of the most important tasks in magnetic anomaly interpretation is the estimation of the model parameters of causative source bodies. The quantitative interpretation of magnetic anomalies generally involves estimations of source positions

^{*} A part of this paper was presented as an abstract at the 2nd International Conference on Civil and Environmental Engineering, 8–10 May 2017, Cappadocia-Nevşehir (Turkey).

(depth and exact origin), shape factor (source geometry) and magnetization contrast (Parasnis 1986, Srivastava and Agarwal 2010, Biswas 2016). The common approach to achieve this task is to perform an efficient inversion procedure. However, as it is well-known, the non-unique, non-linear and ill-posed nature of the magnetic anomaly inversion makes the processing and interpretation more difficult. Moreover, in linear problem cases, the existence of lesser number of known quantities than the number of unknown geological model parameters mostly causes an inherent ambiguity which makes the interpretation more complicated (Roy 1962, Srivastava and Agarwal 2010). Thus, the inversion problem of magnetic anomalies strongly requires some constraints and *a priori* information in order to recover interpretable and realistic model parameter solutions describing the geological source (Li and Oldenburg 1996, 2003, Fedi and Rapolla 1999, Portniaguine and Zhdanov 2002, Morris *et al* 2007, Shamsipour *et al* 2011, Bektaş *et al* 2013, Cheyney *et al* 2015). The other important issue to be considered is the existence of remanent magnetization (Roest and Pilkington 1993, Dannemiller and Li 2006, Lelievre and Oldenburg 2009). Remanent magnetization generally produces noteworthy effects and alters the total magnetization direction of the source, which may lead to incorrect interpretations if ignored (Telford *et al* 1990, pp 106, Shearer and Li 2004, Srivastava and Agarwal 2010, Ekinci 2016). Except for the conventional three-dimensional (3D) non-linear inversion schemes which recover the magnetization magnitude by inverting the amplitude of the anomalous magnetic vector (e.g. Bhattacharyya 1980, Rao and Babu 1991, Balkaya *et al* 2017), most of the inversion techniques generally assume that the direction of the source body magnetization is parallel to the ambient field, namely, to Earth's magnetic field (e.g. Li and Oldenburg 1996, Fregoso and Gallardo 2009, Shamsipour *et al* 2011). This assumption mostly causes to obtain unstable and unrealistic model parameters in the existence of considerable remanent magnetization. In order to overcome this problem, analytic signal amplitude (ASA) of the observed magnetic anomaly can be used (Srivastava and Agarwal 2010). On the contrary to the 3D case (Keating and Sallahac 2004, Shearer and Li 2004, Chen *et al* 2009), the complexities do not exist in the two-dimensional (2D) ASA of the magnetic anomaly which is independent of both ambient field direction and the direction of magnetization of the source body (Nabighian 1972). Thus, the procedure easily allows for model parameter estimations from the response of a causative body without *a priori* information of both ambient field and magnetization direction.

Srivastava and Agarwal (2010) have showed the applicability of particle swarm optimization (PSO) being a population-based metaheuristic algorithm for the inversion of synthetic and real magnetic anomalies via the ASA approach. The PSO algorithm is the most frequently used metaheuristic in recent years for the inversions of geophysical data sets (e.g. Shaw and Srivastava 2007, Fernández-Martínez *et al* 2010, Monteiro Santos 2010, Pekşen *et al* 2011, 2014, Göktürkler and Balkaya 2012, Tronicke *et al* 2012, Pallerio *et al* 2015, Ekinci 2016, Singh and Biswas 2016). In addition to the PSO, various population-based evolutionary optimization algorithms such as the genetic algorithm (Boschetti *et al* 1996, Başoğur *et al* 2007, Balkaya

et al 2012, Göktürkler and Balkaya 2012), ant colony optimization (Srivastava *et al* 2014, Liu *et al* 2015), differential evolution (DE) (Li and Yin 2012, Balkaya 2013, Yu *et al* 2014, Ekinci *et al* 2016, Balkaya *et al* 2017), firefly (Zhou *et al* 2014), differential search (Song *et al* 2014) and hybrid genetic-price (Di Maio *et al* 2016) have been used for parameter estimation problems from a variety of geophysical data sets. Additionally, apart from the population-based evolutionary optimization algorithms, a single state stochastic optimization algorithm, namely simulated annealing (SA) has a range of applications in geophysical inverse problems (Göksu *et al* 2005, Göktürkler 2011, Sharma and Biswas 2011, Göktürkler and Balkaya 2012, Biswas and Sharma 2014, 2015). The main advantage of using one of the metaheuristics given above is that they do not require gradient information for the problem to be optimized. Also, since these algorithms are designed to search optimal solutions by taking into account relatively large parameter intervals in the search space, there is no notable effect of initial model parameter values on the solution. Of the global optimization algorithms mentioned above, the DE optimization algorithm (Storn and Price 1995, Price *et al* 2005, Storn 2008) is an efficient stochastic vector-based metaheuristic algorithm and widely used to solve real-valued numerical optimization problems as reported in detail by Qing (2009, pp 41–51). However, except for a few publications emphasized above there is no other study on the inversion of potential field anomalies using the DE algorithm.

In this study, inversion studies via DE algorithm were performed using both synthetically produced data with and without noise, and the field data sets including both small- and large-scale magnetic profile anomalies caused by an iron deposit (Kesikköprü-Bala, Turkey) and a deep-seated magnetized structure (Sea of Marmara, Turkey), respectively. Moreover, the results determined using DE optimization were compared with those obtained from the well-established magnetic anomaly interpretation techniques, namely, normalized full gradient (NFG) and Euler deconvolution (EUL) techniques.

2. Methodology

Nabighian (1972) has showed that the 2D ASA of a magnetic anomaly profile can be given by

$$|\text{ASA}(x)| = (V_x^2 + V_z^2)^{1/2} \quad (1)$$

where V_x and V_z are the horizontal and vertical derivatives of the magnetic anomalies, respectively. Additionally, 2D ASA of some idealized causative body geometries can be approximated by the following generalized equation (Nabighian 1972, Thurston and Smith 1997, Salem *et al* 2004, Salem 2005)

$$|\text{ASA}(x)| = \frac{A}{[(x - x_0)^2 + z_0^2]^q} \quad (2)$$

where A is the amplitude coefficient related to the physical properties of the source, q is the shape factor related to the geometry of the source, x_0 and z_0 denote the exact origin and depth to the top of the causative body, respectively. Over a contact, a thin dike and a horizontal cylinder the shape factors as 0.5, 1 and 1.5 are used, respectively (Srivastava and

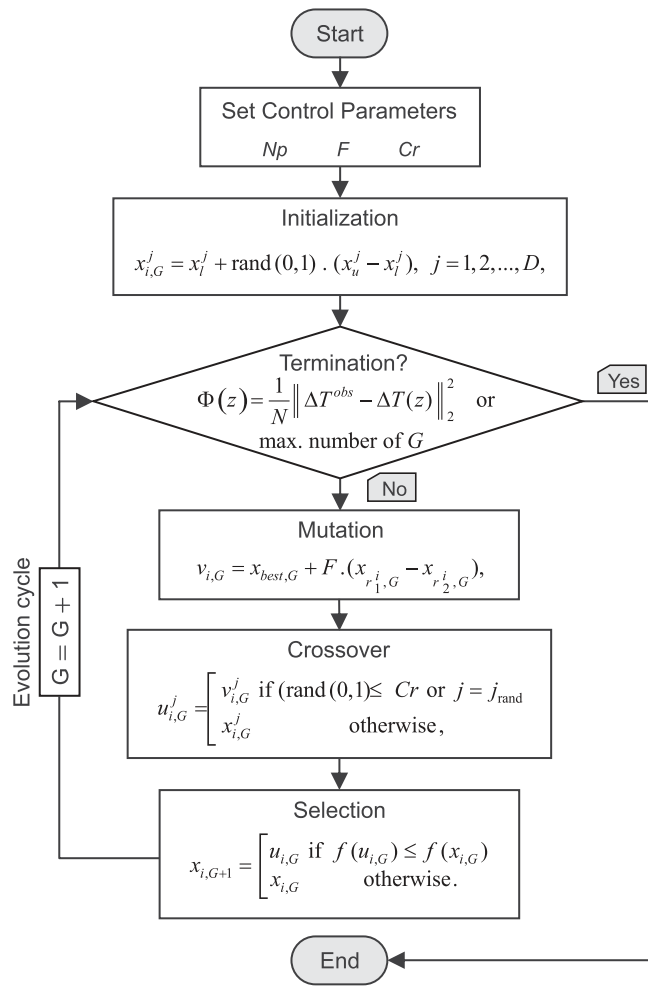


Figure 1. A simple flowchart of the DE algorithm.

Agarwal 2010). An inversion scheme via DE algorithm can be adapted using equation (2) for model parameter estimation from the anomalies of magnetized bodies. The methodologies of the techniques used here are given in brief in the following subsections.

2.1. DE algorithm

A simplified flowchart for DE being a derivative-free and vector-based metaheuristic is given in figure 1. The algorithm has user-defined and algorithm-dependent control parameters like the almost all population-based metaheuristics. These control parameters consisting of crossover probability (Cr), mutation scale factor (F) and population size (Np) can greatly affect the success, performance and convergence characteristic of the algorithm (Yang 2014, p. 38). Even though the number of generations (G_{max}) is not taken into consideration as a control parameter some stopping criteria can be used. Therefore the stopping criteria should be set to an optimal value to reduce elapsed time during the optimization (Peñuñuri et al 2016). As can clearly be seen from the flowchart, initialization stage and evolution cycle by genetic operators (i.e. mutation, crossover and selection) are two

essential parts of DE. In the algorithm, initial population vectors representing individual solutions are randomly generated within a predefined search space considering the upper and lower bounds of each parameter as presented in the flowchart. Evolution of solutions is then achieved by some genetic operations mentioned above via equations given in the flowchart until a predefined termination criterion (i.e. error energy, $f(x)$ and/or maximum number of G) is met. Thus, the vector providing the lower $f(x)$ value is selected as an optimal solution for the optimization problem under consideration (Price et al 2005, p. 30). In this study, among the strategies in DE algorithm, an elitist strategy, namely, DE/best/1/bin was used which yields better results with a good accuracy and less computational cost for the inversion of low-dimensional geophysical data sets (Balkaya 2013). During the operations base vector is chosen to be the best vector of the current generation, there is only a pair of differential vectors and a binomial crossover is used. More details for the algorithm and notations related to equations mentioned in figure 1 can be found in previous papers of DE applications in geophysical problems (e.g., Balkaya 2013, Ekinci et al 2016, Balkaya et al 2017).

2.2. NFG technique

The NFG technique, based on the downward continuation and ASA, has been proved useful in the determination of the source positions and depths using potential field anomalies (Zeng et al 2002, Aydin 2007, Oruç and Keskinsezer 2008, Sındırgı et al 2008, Ekinci and Yiğitbaş 2012, 2015, Sheng and Xiaohong 2015). The 2D NFG amplitude at a specific point is given as (Berezkin 1967, 1973)

$$NFG(x, z) = \frac{[V_x^2(x_i, z_j) + V_z^2(x_i, z_j)]^{1/2}}{\frac{1}{M} \sum_{i=1}^M [V_x^2(x_i, z_j) + V_z^2(x_i, z_j)]^{1/2}} \quad (3)$$

where $NFG(x, z)$ is the NFG amplitude, M represents the number of the data, z_j is the downward continuation level. The denominator of equation (3) is the mean value of ASA, and this normalization makes the NFG amplitude dimensionless. If the potential field data are defined in the positive x -axis (0, L) only the sine expansion is used (Rikitake et al 1976) and the downward continuation process can be obtained using Fourier series summation as follows (Jung 1961)

$$V(x, z) = \sum_{n=1}^N \left[B_n \sin\left(\frac{\pi nx}{L}\right) \right] e^{\pi nz/L} \quad (4)$$

where B_n is the Fourier sine coefficient, z represents the downward continuation level and n is the harmonic number. The coefficient B_n is obtained by

$$B_n = \frac{1}{L} \int_{-L}^L V(x, 0) \sin\left(\frac{\pi nx}{L}\right) dx. \quad (5)$$

First-order horizontal and vertical derivatives of the function $V(x, z)$ are defined as follows (Berezkin 1988)

$$\partial V_x(x, z) = \frac{\pi}{L} \sum_{n=1}^N n B_n \cos\left(\frac{\pi n x}{L}\right) e^{\pi n z/L} q \quad (6)$$

$$\partial V_z(x, z) = \frac{\pi}{L} \sum_{n=1}^N n B_n \sin\left(\frac{\pi n x}{L}\right) e^{\pi n z/L} q \quad (7)$$

where

$$q = \left[\sin\left(\frac{\pi n}{N}\right) / \frac{\pi n}{N} \right]^\mu \quad (8)$$

where q is the Lanczos smoothing term used to eliminate the Gibbs effect resulting from downward continuation process (Berezkin 1967), and μ represents the degree of smoothing which controls the curvature of the Lanczos smoothing term. In the NFG technique, some values in an increasing order are tried to find the optimum harmonic intervals (Dondurur 2005, Aydin 2007). The procedure produces closed contours around the causative body for all harmonic limits but the centre of fully closed symmetric contours showing the main local maximum mostly indicate the actual depth and the exact origin of the source (Aydin 2007, Sındırgı et al 2008). Here, optimal limit values of the harmonics were determined by trial-and-error and the solutions of every example were illustrated using two NFG sections which include the optimum one.

2.3. EUL technique

The EUL technique is used to estimate the exact origin and the depth of the potential field source using the Euler's homogeneity relation (Thompson 1982). This technique uses first-order horizontal and vertical derivatives of the data and is based on the use of Euler's homogeneity equation on a moving data window with a given structural index (SI), which is related to the nature and geometry of the source body (Gerovska and Arauzo-Bravo 2003, Dewangan et al 2007, Zunino et al 2009, Ekinici et al 2014). In the computation procedure, a set of normal equations are solved by assuming the geometry of magnetic source, namely, SI (Stavrev 1997, Durrheim and Cooper 1998, Doo et al 2007, Srivastava and Agarwal 2010, Rabeh and Khalil 2015). Euler's equation for profile data is given as follows (Thompson 1982)

$$(x - x_0) \frac{\partial \Delta T}{\partial x} - z_0 \frac{\partial \Delta T}{\partial z} = -N \Delta T(x). \quad (9)$$

Rearrangement of equation (9) yields (Thompson 1982)

$$x_0 \frac{\partial \Delta T}{\partial x} + z_0 \frac{\partial \Delta T}{\partial z} = x \frac{\partial \Delta T}{\partial x} + N \Delta T(x) \quad (10)$$

where ΔT denotes the observed magnetic field at (x, z) , x_0 and z_0 are the exact origin and the depth of the source body, the degree of homogeneity N represents the SI (Thompson 1982), which is also a measure of the rate of change with distance of a field (Reid et al 1990). $\partial \Delta T / \partial x$ and $\partial \Delta T / \partial z$ are the first-order horizontal and vertical derivatives calculated from the observed total field ΔT . It is known that

irregular sill like bodies, dikes and faults with limited throw can be best displayed by an SI of 1 (Reid et al 1990). Considering the synthetic models and the solutions obtained by DE, we used an SI of 1 for EUL on both synthetic and real data examples.

3. Synthetic examples

The validity and robustness of DE algorithm were tested in the estimation of the model parameters (i.e. A , x_0 , q and z_0) of source bodies using ASAs of synthetically produced noise-free and noisy anomalies. Tests studies were performed using some different hypothetic models including single (Model 1) and multiple source bodies (Models 2 and 3). Total field magnetic anomaly (TMA) due to a thin sheet or a dike can be computed from the equations derived by Nabighian (1972) as follows

$$T(x) = A \frac{z_0 \cos \varphi + x \sin \varphi}{(x - x_0)^2 + z_0^2} \quad (11)$$

where

$$A = 2 k F (1 - \cos^2 i \sin^2 D) \sin d \quad (12)$$

$$\varphi = 2 I - d - 90 \quad (13)$$

$$I = \arctan(\tan i / \cos D) \quad (14)$$

where k is the susceptibility contrast, F represents the Earth's magnetic field, i is the inclination of Earth's field, z_0 denotes the depth to the top of the body, d is the dipping angle, D is the angle between magnetic north and positive x -axis, x_0 is the exact origin of the causative body, x represents the horizontal position coordinates on the profile. Here, A can be considered as the amplitude related to the physical properties of the source body. In all synthetic applications, TMAs were produced using the model parameters $i = 60^\circ$, $D = 0^\circ$ and $d = 90^\circ$. Additionally, ASAs of synthetic TMAs were computed using frequency domain filtering operations via fast Fourier transform as described by Agarwal and Srivastava (2008).

3.1. Single thin dike (model 1)

Synthetic TMA response of a single thin dike model was generated using equation (11) with the model parameters $z_0 = 5$ m, $x_0 = 50$ m and $A = 800$ nT m⁻¹, and assuming 1 m sampling interval (figure 2 upper left panel). The produced anomaly was also corrupted with normally distributed zero-mean pseudo-random numbers. The different percentages of noise levels (i.e. 3, 5, 8 and 10) were added by scaling the original data. Synthetic TMA having 10% of noise level is demonstrated in figure 2 (lower left panel). ASAs of these noise-free and noisy TMAs are shown in figure 2 (right panels) with red circles.

Before the inversion studies, the convergence and the parameter resolution characteristics were analysed by producing some prediction error maps for each pair of the model parameters by setting the rest of the parameters to the true values and using a relatively narrower search spaces (Balkaya 2013, Ekinici et al 2016). In order to perform these significant

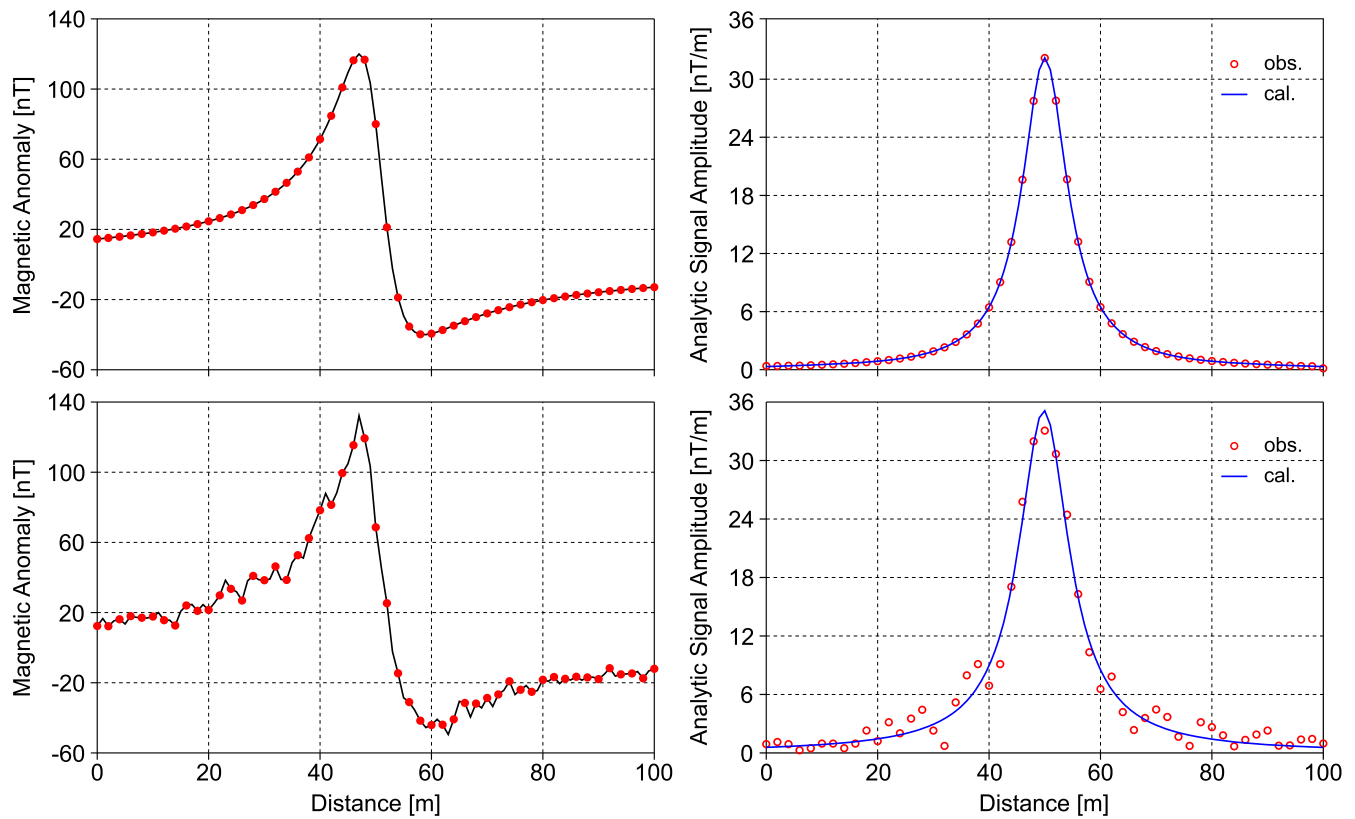


Figure 2. TMA of Model 1 (upper left panel) and its contaminated form by 10% noise level (lower left panel). ASA inversion results of noise-free TMA (upper right panel) and noisy TMA (lower right panel). Note that red circles are located every two meters.

analyses, equation (2) was used for the forward modelling procedure. White circles in the error maps show the true values for the parameter pairs, and the axes values indicate search space bounds for each model parameter (figure 3). The topographies in these error images clearly illustrated the nature of the inverse problem under consideration. The behaviour of nearly circular closing contours surrounding the global minima for the pairs of $A-x_0$, z_0-x_0 and $q-x_0$ showed that these model parameters are uncorrelated with each other and most likely resolvable independently using an efficient inversion technique. Elliptical contours sloping to the error energy axes are clearly seen from the map of A versus z_0 . This feature points a positive correlation, namely, an increase in a parameter also increases the other one. Similar elliptical contours but indicating a negative correlation are evident in the error map of z_0 versus q (figure 3) which means that an increase in a parameter decreases the other one. On contrary to the parameter pairs mentioned above, unclosed contours and a narrow valley topography in the vicinity of global minimum are easily seen for the pair of $A-q$. Although the contour lines seem nearly parallel to the A axis, gentle sloping contours suggest a positive correlation between these parameters. Thus, there may be many equivalent solutions within the same error limits. Nevertheless, the contour lines lying approximately parallel to the A axis imply that the probability of solving q successfully is higher than the parameter A . Considering the produced prediction error maps for each pair of the parameters, it is avowable that the depth, shape and exact origin of the causative body can be estimated

substantially through the amplitude inversion of 2D analytical signal of a TMA.

In the second stage, considering the synthetic ASA given in figure 2 (upper right panel), some parameter tuning studies relying mainly on choosing optimum control parameters (i.e. F , Cr and Np) were carried out to increase the efficacy of the metaheuristic. First, we investigated the effects of F and Cr pair on the solution. Relatively large search spaces presented in table 1 were used for the model parameters. Table 2 shows the results obtained through the analysis of rms values produced by using various F versus Cr values at the end of 30 independent runs. As clearly seen from the table, the best statistical results were obtained by using the values F of 0.5 versus Cr of 0.9. Additionally, considering these values, we statistically analysed the Np parameter using 10, 15, 20 and 30 times of D (number of unknown parameters), respectively for the synthetic noise-free case. Table 3 shows a brief presentation of the results obtained at the end of 30 independent runs of the algorithm. A threshold value (i.e. 1×10^{-8}) defined as VTR (value to reach) in the algorithm was also used. The algorithm was terminated when the error energy value dropped below the VTR between the two successive generations or G_{max} reached 100.

Considering the minimum, mean and standard deviation of rms values presented in table 3, the highest Np value (i.e. 120) provided better statistical results than the others. It is quite obvious that more generations affect the mean function evaluation and total elapsed time. However, because the anomaly equation used in our case does not need a high

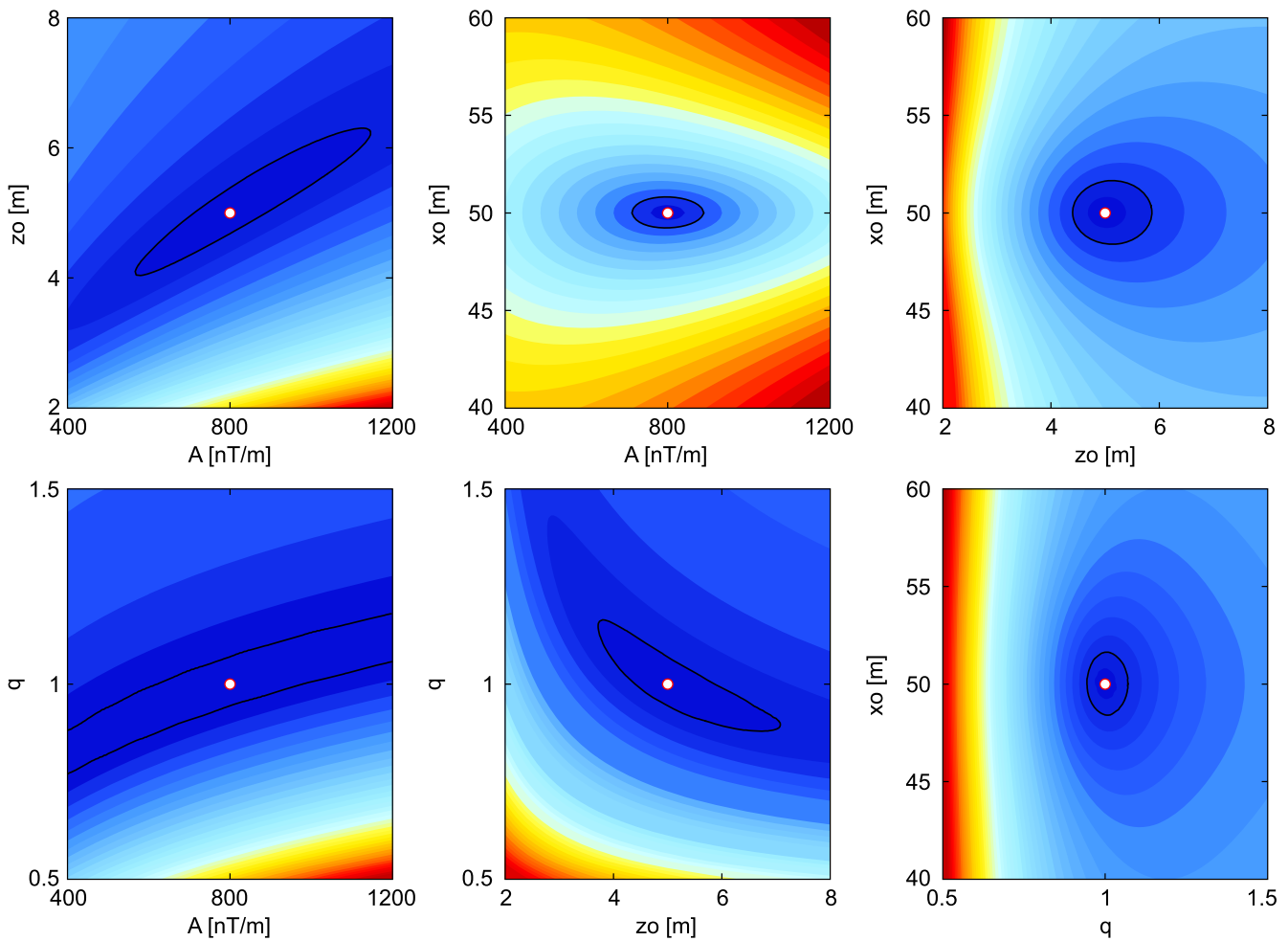


Figure 3. Error energy maps for parameter pairs of noise-free synthetic data case. White circles in each map indicate the true solution. Axes values indicate search space bounds for each model parameter.

Table 1. True and search space parameters of Model 1.

Parameters	True	Search space	
		Minimum	Maximum
A [nT m ⁻¹]	800	1	5000
z_0 [m]	5	1	20
x_0 [m]	50	1	100
q	1	0.2	2

computation time during the optimization, the N_p value was set to 30 D i.e. 120 for the applications. Additionally, based on the parameter tuning results mentioned above, we also set the control parameters as F : 0.5, Cr : 0.9.

After determining the best control parameters for our problem, ASAs of synthetic TMAs having various percentages of noise content were inverted using wider search space bounds given in table 1. Considering the estimated model parameters (table 4), it can be concluded that DE algorithm yielded satisfactory results except for the parameter A even in the existence of various noise contents. Furthermore, these reasonable solutions obtained through the inversions clearly substantiate the results of prediction error maps (figure 3). As

mentioned previously, prediction error maps indicated that the parameters z_0 , x_0 and q are most likely resolvable. The inversion results illustrating the fit between noise-free data and the one having the highest noise content (i.e. 10%) are also shown in figure 2 (right panels). The fits between the synthetic and calculated ASAs generated using the actual and the best-estimated parameters, respectively are quite good.

The inversion results were also compared to those of the NFG and EUL techniques (figure 4). After some trial-and-error applications, an optimum N value was determined for the NFG procedure. In order to show the effect of the selection of optimum harmonic interval, two NFG sections are shown in figure 4 (upper panels). It is obvious that fully closed symmetric contours showing the main local maximum (white circle) indicated the exact solutions with the help of optimum N value (upper right panel in figure 4). Satisfactory solutions were also obtained via the EUL technique, although to a lesser extent than for the NFG technique (figure 4 lower panel). When considering the noisy data case (figure 5), the NFG technique produced reasonable model parameters like the DE algorithm. On the other hand, the EUL technique partially meets the expectations in this case.

Table 2. The best minimum (top), mean (middle) and standard deviation (bottom) results of *rms* values obtained from parameter tuning studies considering various *F* and *Cr* values for DE algorithm. The best statistical results are shown in boldface type (i.e., *F* = 0.5 and *Cr* = 0.9).

Cr	F								
	0.1	0.2	0.3	0.4	0.5	0.6	0.7	0.8	0.9
0.1	0.34	0.33	0.75	0.58	1.35	0.83	1.17	0.71	1.49
	1.94	1.32	1.84	1.54	1.98	2.24	2.02	2.50	2.45
	0.97	0.61	0.55	0.82	0.48	0.96	0.76	1.08	0.67
0.2	0.19	0.18	0.17	0.25	0.37	0.28	0.56	0.77	0.71
	1.38	0.27	0.40	0.66	0.93	1.19	1.30	1.22	1.69
	1.04	0.09	0.13	0.29	0.39	0.60	0.54	0.54	0.77
0.3	0.16	0.16	0.16	0.16	0.21	0.17	0.33	0.24	0.43
	1.55	0.20	0.25	0.24	0.45	0.40	0.59	0.98	0.85
	1.44	0.06	0.17	0.08	0.17	0.14	0.21	0.40	0.39
0.4	0.16	0.16	0.16	0.16	0.17	0.26	0.21	0.37	0.39
	0.51	0.25	0.31	0.17	0.27	0.38	0.48	0.63	0.84
	0.62	0.25	0.46	0.02	0.12	0.11	0.22	0.20	0.29
0.5	0.16	0.16	0.16	0.16	0.16	0.17	0.16	0.24	0.25
	2.13	0.41	0.17	0.16	0.16	0.21	0.27	0.44	0.61
	1.17	0.40	0.04	0.01	0.01	0.03	0.08	0.20	0.25
0.6	0.16	0.16	0.16	0.16	0.16	0.16	0.17	0.17	0.25
	1.45	1.13	0.16	0.16	0.16	0.17	0.20	0.29	0.48
	1.10	1.27	5×10^{-6}	2×10^{-4}	3×10^{-3}	8×10^{-3}	0.03	0.10	0.14
0.7	0.19	0.16	0.16	0.16	0.16	0.16	0.16	0.17	0.19
	1.63	1.66	0.16	0.16	0.16	0.16	0.18	0.23	0.39
	1.12	1.16	1.1×10^{-5}	1×10^{-5}	9×10^{-5}	4×10^{-3}	0.02	0.07	0.14
0.8	0.16	1.28	0.16	0.16	0.16	0.16	0.16	0.16	0.18
	1.83	2.49	1.30	0.27	0.16	0.16	0.17	0.18	0.21
	1.20	0.87	1.06	0.34	7×10^{-6}	2×10^{-4}	0.05	0.02	0.03
0.9	1.12	1.09	0.16	0.16	0.16	0.16	0.16	0.16	0.16
	3.47	2.54	0.64	0.81	0.16	0.16	0.16	0.17	0.23
	1.30	0.80	0.70	0.86	1×10^{-6}	1×10^{-5}	9×10^{-4}	0.01	0.07

Table 3. The best statistical results obtained from DE algorithm for the noise-free Model 1 case considering four different values of *Np* at the end of 30 independent runs (*F* = 0.5, *Cr* = 0.9).

Statistics		<i>Np</i>			
		40	60	80	120
<i>rms</i> [nT m ⁻¹]	min.	0.02	0.02	0.02	0.02
	mean	0.11	0.05	0.04	0.03
	std. dev.	0.12	0.04	0.04	1×10^{-4}
<i>G</i>	mean	80.87	77.1	77.47	65.7
	std. dev.	26.17	28.66	27.77	22.45
Function evaluation	mean	3234	4620	6197	7884
	std. dev.	1046.91	1719.37	2211.47	2693.84
Total elapsed time [s]		46	53	61	72

3.2. Two thin dikes (Models 2 and 3)

Using the model parameters given in table 5, a synthetic TMA caused by two thin dikes (Model 2) was produced (figure 6 upper left panel) to test the performance of DE algorithm. In the

evaluation, the same best control parameters given previously were used. The computed ASA of the TMA is demonstrated in the related panel of the figure. Search space bounds and the estimated parameters through the inversion are given in table 5.

Table 4. True and estimated parameters of Model 1.

Parameters	True	Noise content				
		0%	3%	5%	8%	10%
A [nT m ⁻¹]	800	782.41	730.19	1215.69	1311.19	612.75
z ₀ [m]	5	4.98	4.98	5.73	5.69	5.28
x ₀ [m]	50	50.01	50.09	50.09	50.03	49.83
q	1	1	0.98	1.06	1.08	0.91
rms [nT m ⁻¹]		0.02	0.43	0.53	0.73	0.90

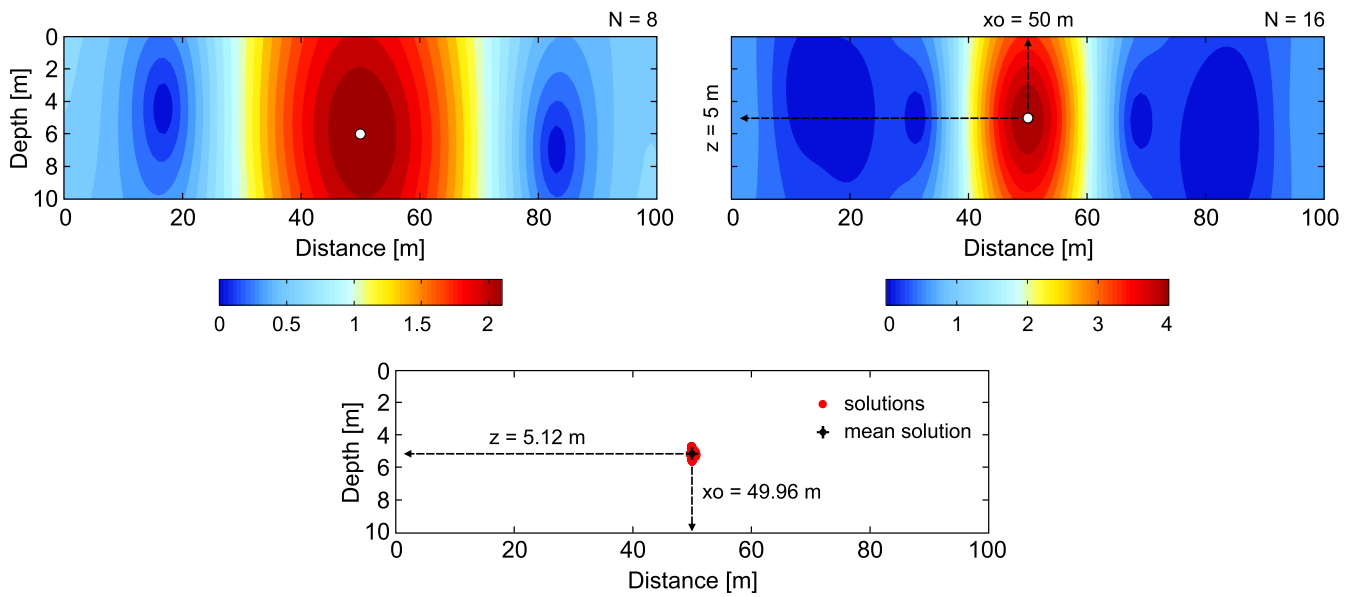


Figure 4. NFG sections (upper panels) and EUL solutions (lower panel) obtained from the TMA response of Model 1 (figure 2 upper left panel). Note that optimum value of N was found to be 16 for NFG computation.

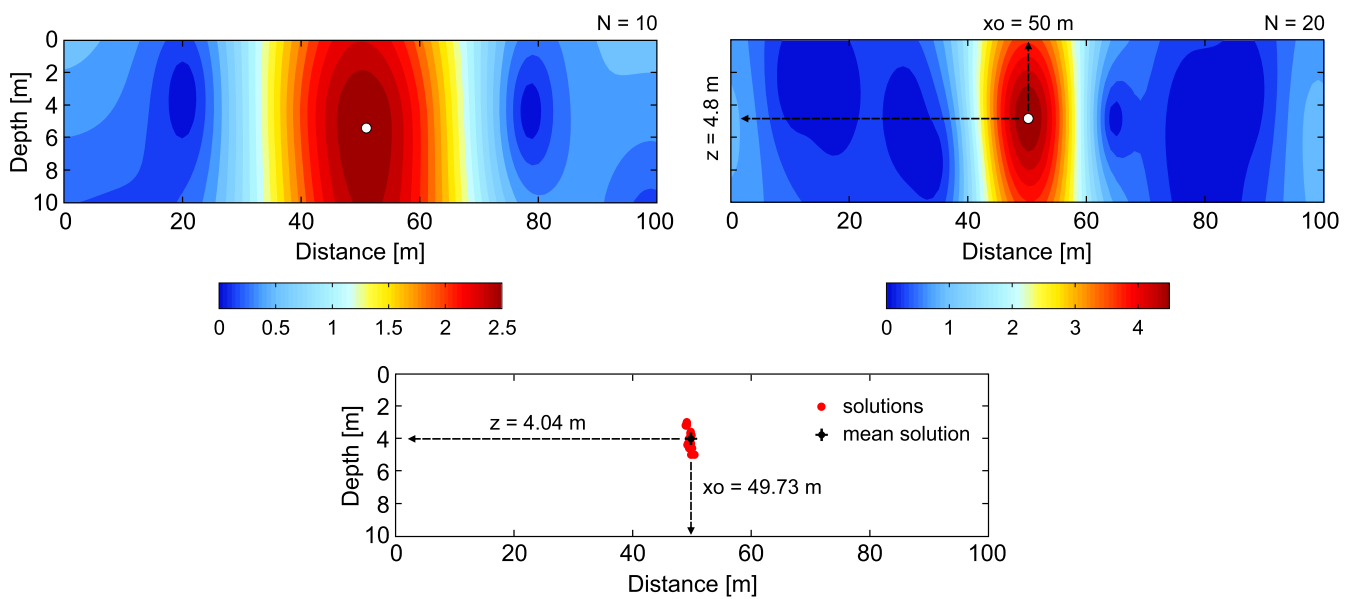


Figure 5. NFG sections (upper panels) and EUL solutions (lower panel) obtained from the noise-added response of Model 1 (figure 2 lower left panel). Note that optimum value of N was found to be 20 for NFG computation.

Table 5. True parameters, search spaces and estimated parameters of Model 2 and Model 3 through DE algorithm.

Case	Bodies	Parameters	True parameters	Search space		Estimated parameters
				Minimum	Maximum	
Model 2	First	A [nT m^{-1}]	800	1	5000	791.94
		z_0 [m]	5	1	20	5.01
		x_0 [m]	30	1	50	29.92
		q	1	0.2	2	1.01
	Second	A [nT m^{-1}]	1000	1	5000	1042.54
		z_0 [m]	4	1	20	4.04
		x_0 [m]	70	50	100	70.04
		q	1	0.2	2	1.01
		rms [nT m^{-1}]				0.15
	Model 3	First	A [nT m^{-1}]	800	1	5000
z_0 [m]			5	1	20	5.09
x_0 [m]			42	1	50	42.05
q			1	0.2	2	1.07
Second		A [nT m^{-1}]	1000	1	5000	1129.05
		z_0 [m]	4	1	20	4.05
		x_0 [m]	58	50	100	57.97
		q	1	0.2	2	1.03
		rms [nT m^{-1}]				0.02

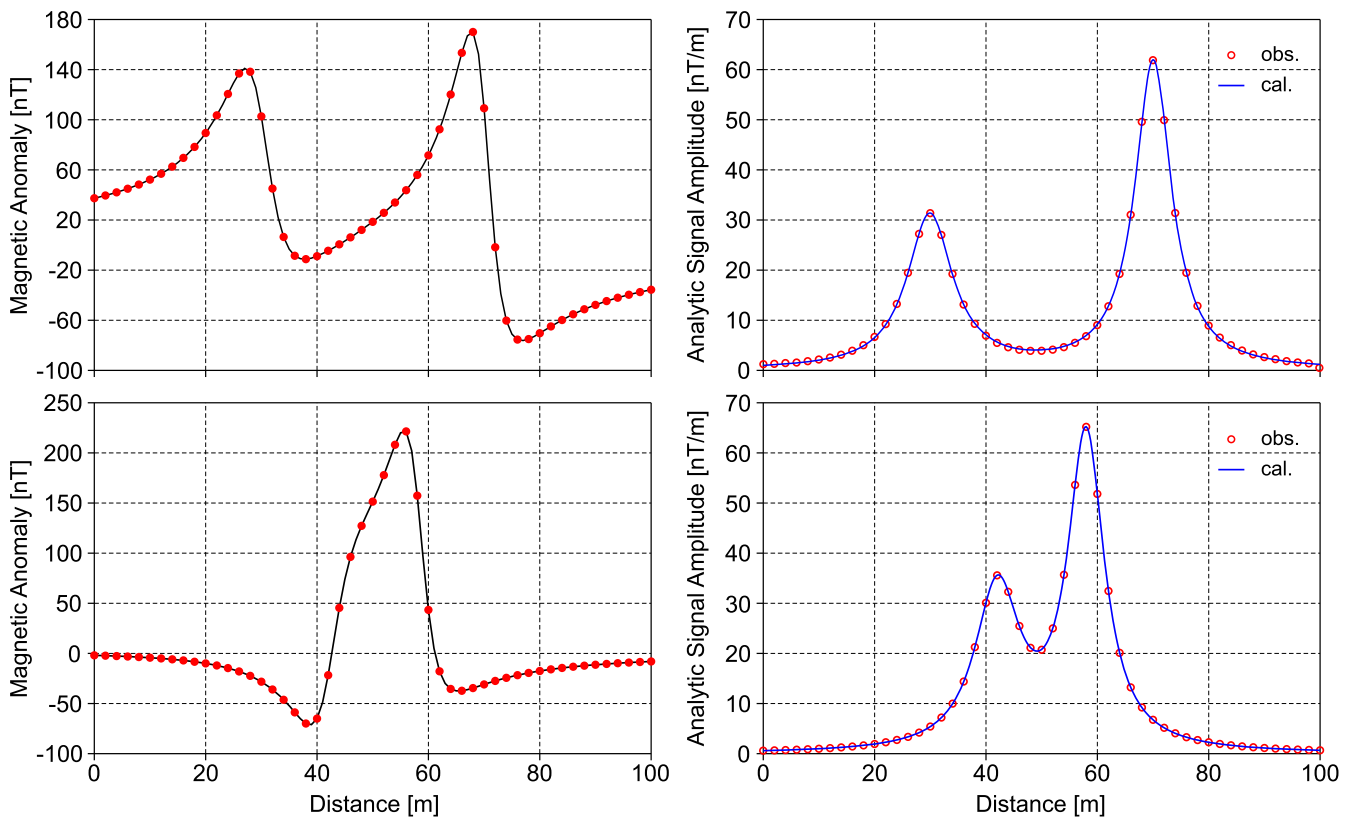


Figure 6. TMAs of Model 2 (upper left panel) and Model 3 (lower left panel). ASA inversion results of Model 2 (upper right panel) and Model 3 (lower right panel).

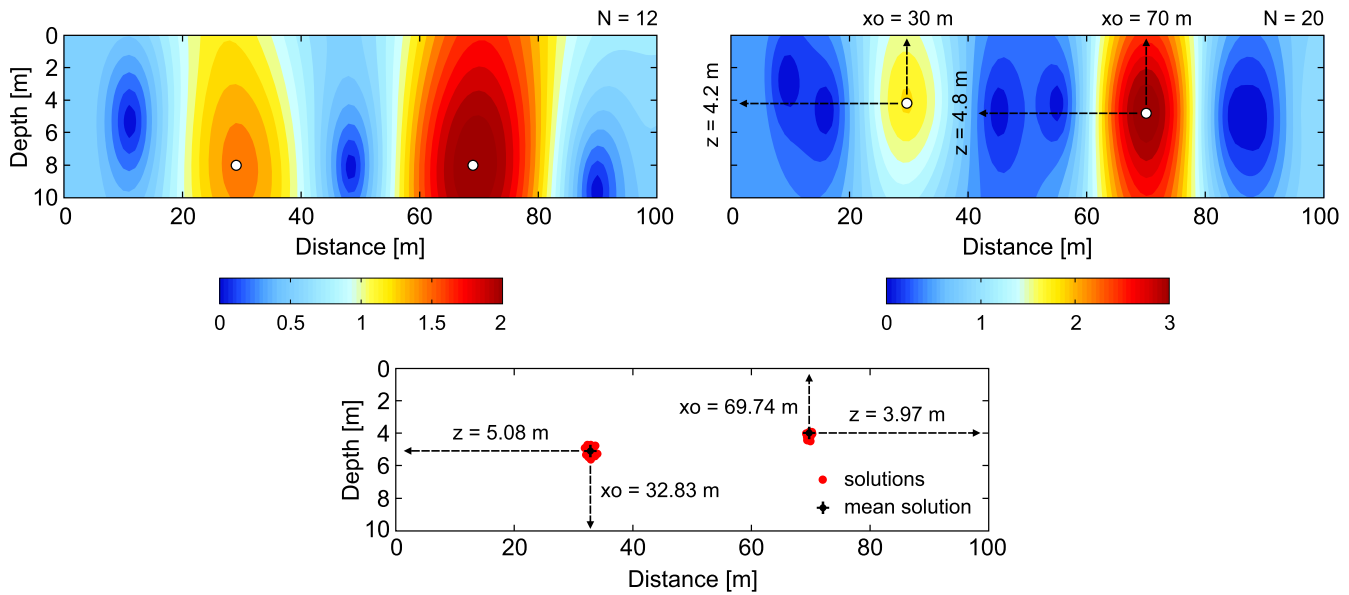


Figure 7. NFG sections (upper panels) and EUL solutions (lower panel) obtained from the response of Model 2 (figure 6 upper left panel). Note that optimum value of N was found to be 20 for NFG computation.

Table 6. The best statistical results obtained from the DE algorithm for the TMAs of Model 2 and 3 at the end of 30 independent runs ($Np = D \times 30$).

Statistics		Model 2	Model 3
rms [$nT\ m^{-1}$]	min.	0.15	0.02
	mean	0.38	1.34
	std. dev.	0.79	2.29
G	mean	99.73	98.03
	std. dev.	1.46	7.49
Function evaluation	mean	111 968	117 64
	std. dev.	175.27	899.37
Total elapsed time [s]		157	138

DE optimization revealed a pleasing agreement between the synthetic and calculated ASAs (figure 6 upper right panel). The best statistical results for Model 2 (table 6) showed that very small rms errors ($<1\ nT\ m^{-1}$) were obtained at every independent run. Additionally, independent runs were terminated by the nearly same number of generations, indicating the stability of the inversion algorithm in this case. The solutions obtained through the NFG and EUL techniques for Model 2 are illustrated in figure 7. On contrary to the solutions obtained from the noisy data of Model 1, the NFG solutions could not fulfil the expectations for Model 2. In this instance, the EUL solutions are more successful than those of the NFG technique. However, it must be noted that the closest model parameters to the actual ones were achieved via the DE algorithm.

In the next simulation, a more complicated TMA (Model 3) having interference from a neighbouring causative source was analysed to test the efficacy of the DE optimization. In this case, we used two thin dikes having opposite polarities, and we also reduced the distance between the sources to get a

complex TMA (figure 6 lower left panel). The true parameters of each causative body are given in table 5. It is clearly seen from the produced TMA that the anomaly pattern does not seem to be caused by multiple sources at first sight. However, after the ASA computation, the magnetic traces of two anomalous bodies explicitly became visible. This simulation also emphasized the significance of the ASA computation in magnetic anomaly interpretation. Search space bounds and the estimated model parameters through the DE optimization are given in table 5. Although using such a large search space bounds, model parameters were resolved successfully, confirming the robustness and the validity of the algorithm. The good agreement between the synthetic and calculated ASA curves is also demonstrated in figure 6 (lower right panel). Table 6 shows the best statistical results, indicating that low rms values were obtained in each run. Additionally, it was also observed that a maximum number of 100 generations is adequate for the inversion of ASAs due to two causative sources (table 6). The NFG and EUL solutions for this case are shown in figure 8. It is clearly seen that unlike the DE algorithm, these techniques could not provide reasonable results with the multiple bodies located relatively close to each other.

4. Field examples

The efficiency of the DE optimization algorithm was also tested using two field data sets including an iron deposit anomaly in Kesikköprü (Turkey) and a deep-seated magnetized structure anomaly in the Sea of Marmara (Turkey). ASAs of both anomalies were obtained using the method of Agarwal and Srivastava (2008). Since these geological structures causing the TMAs may not be represented by exact idealized subsurface models, the field data sets were inverted without fixing the shape factor to an idealized body to obtain

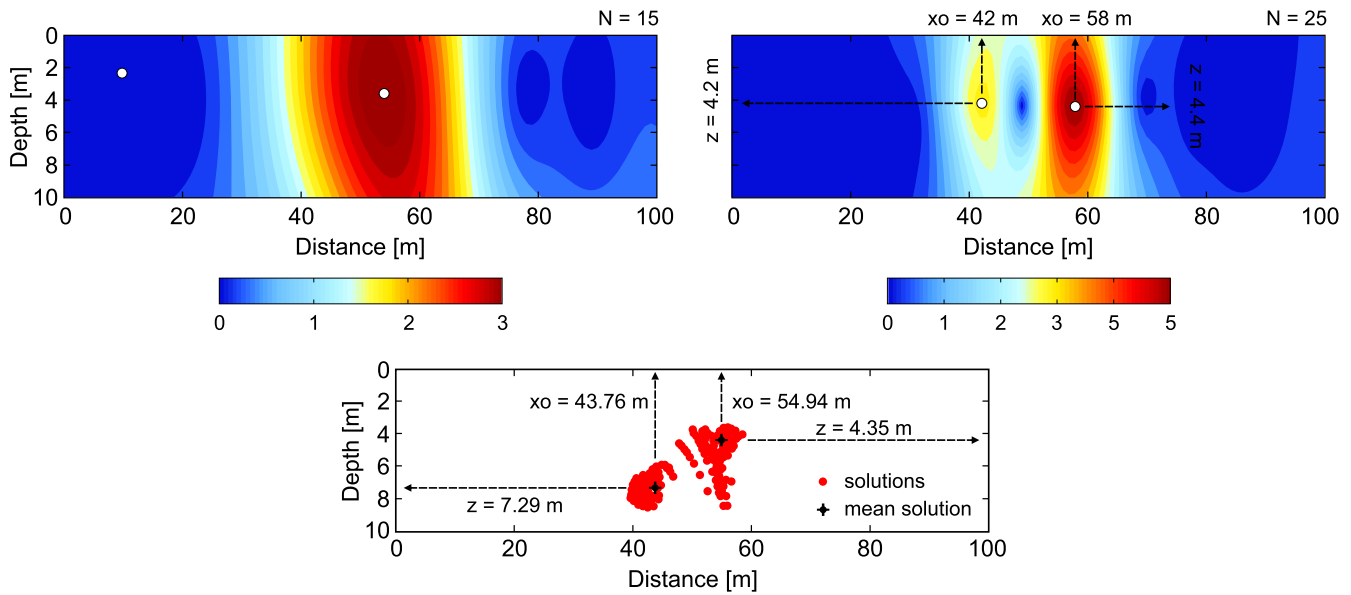


Figure 8. NFG sections (upper panels) and EUL solutions (lower panel) obtained from the response of Model 3 (figure 6 lower left panel). Note that optimum value of N was found to be 25 for NFG computation.

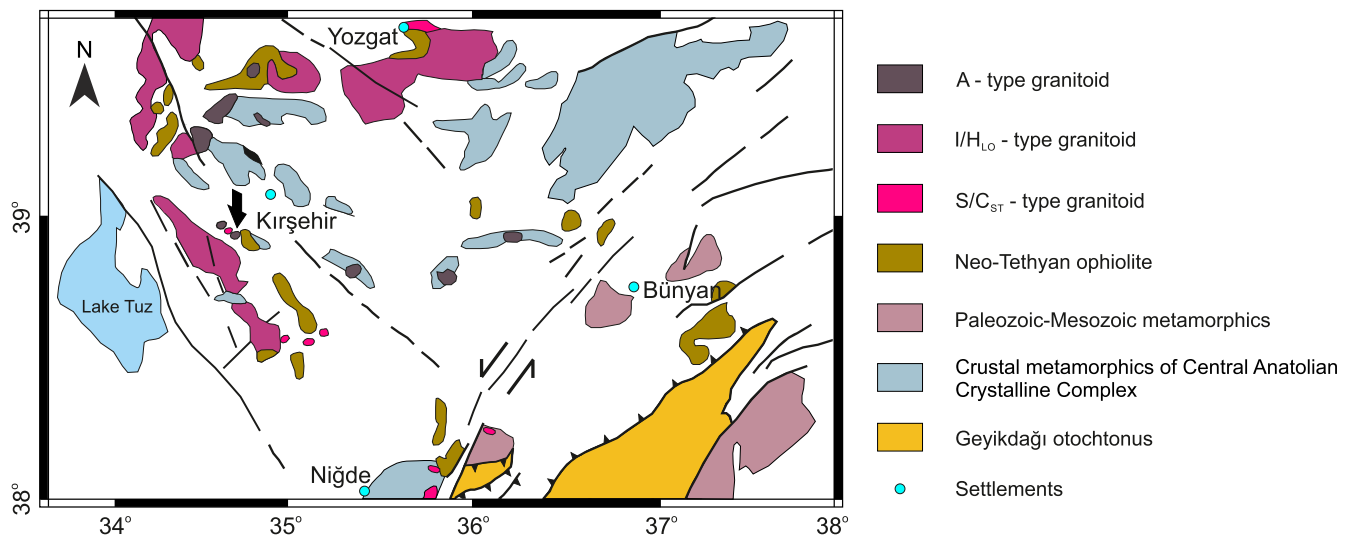


Figure 9. Simplified geographical settings of the plutonic and metamorphic rocks in central Anatolia, Turkey (modified after Bingöl 1989 and Boztuğ 1998). The black arrow shows the Kesikköprü pluton.

possible geometries whose ASAs of magnetic responses are similar to the ASAs of observed data. The same statistical analyses performed in synthetic simulations were also considered. The field anomalies are most likely caused by single causative sources. Since synthetic simulations showed the good performance of the NFG and EUL techniques on a single body model, we also supported the solutions obtained from the DE algorithm with those of the NFG and EUL techniques.

4.1. Kesikköprü iron deposit, Ankara, central Turkey

The first example of real data cases includes a TMA observed over the Kesikköprü iron deposit (Bala-Ankara, Turkey) located in the Central Anatolian Crystalline Complex (figure 9). It is one of the largest iron reserves in Turkey. The

basement is comprised of rock assemblages of the Kirsehir massive, and it is overlain by the upper Cretaceous ophiolitic complex together with sedimentary and volcanic-volcaniclastic rocks and by a sedimentary cover of Tertiary age (Doğan *et al* 1998). The skarn and vein deposits constitute an important part of the metallogeny of the Central Anatolian Crystalline Complex (Kuşcu and Erler 1998). In the region, the skarn-type iron deposits developed immediately adjacent to granitoid contacts (Oruç 2013). The residual TMA acquired by the General Directorate of Mineral Research and Exploration of Turkey (MTA) was compiled for Kesikköprü region (Oruç 2013). The 120 m long residual TMA sampled every 3 m is shown in the left panel of figure 10. Search space parameters used in the DE optimization and the best statistical results obtained at the end of the 30 independent runs are given in tables 7 and 8, respectively. The fit between the

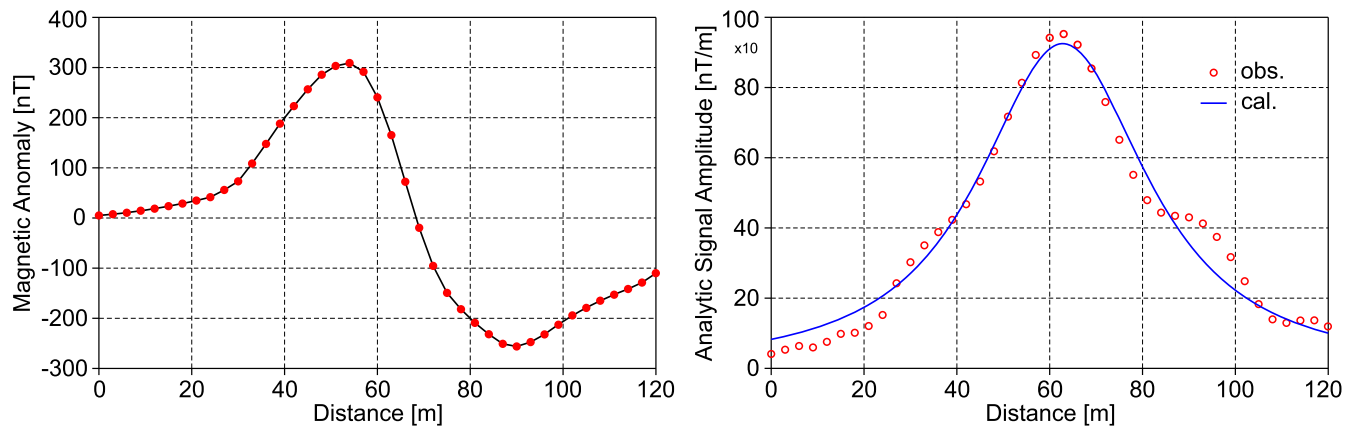


Figure 10. TMA observed over the Kesikköprü iron deposit (left panel) and the fit between the ASAs calculated from the TMA and the response of best-fitting model parameters estimated via the DE algorithm (right panel).

Table 7. Search space parameters for the Kesikköprü and Sea of Marmara TMAs.

Case	Parameters	Search space	
		Minimum	Maximum
Kesikköprü	A [nT m ⁻¹]	1000	1×10^7
	z_0 [m]	1	100
	x_0 [m]	1	120
	q	0.2	2
Marmara	A [nT km ⁻¹]	100	1×10^5
	z_0 [km]	1	10
	x_0 [km]	1	40
	q	0.2	2

Table 8. The best statistical results obtained from the DE algorithm for the Kesikköprü and Sea of Marmara TMAs at the end of 30 independent runs ($N_p = D \times 30$). The unit of rms is nT m⁻¹ for the Kesikköprü anomaly and nT km⁻¹ for the Marmara anomaly.

Statistics		Kesikköprü	Marmara
rms	min.	45.68	5.62
	mean	45.69	5.91
	std. dev.	0.02	0.32
G	mean	91.4	96.13
	std. dev.	17.91	13.03
Function evaluation	mean	109 68	115 36
	std. dev.	2149.54	1563.25
Total elapsed time [s]		79	76

ASAs calculated from the TMA and the best-fitting model response is illustrated in the right panel of figure 10. A dike-like model ($q = 1.19$) having a depth of 24.4 m and an exact origin of 62.9 m over the measuring profile was estimated through the inversion process (table 9). This anomaly was previously studied by Oruç (2013) using continuous wavelet transform. The author reported a point dipole (sphere) for the causative body with a depth of 42 m and an exact origin of

Table 9. Model parameters obtained from the NFG, EUL and DE algorithm for the Kesikköprü and Sea of Marmara TMAs. Note that flight height for the Sea of Marmara TMA was taken into consideration. The depths given are the obtained ones from the sea level.

Case	Model parameter	NFG	EUL	DE
Kesikköprü	A [nT m ⁻¹]	—	—	1825 814.9
	z_0 [m]	22.5	15.87	24.4
	x_0 [m]	60	63.16	62.9
	q	—	—	1.19
Marmara	A [nT km ⁻¹]	—	—	1499.58
	z_0 [km]	3.58	3.52	3.78
	x_0 [km]	19.5	20.56	19.97
	q	—	—	0.79

60 m at abscissa. Although the agreement between the obtained exact origin positions, a shallower depth solution was obtained via DE optimization. The depths and exact origins obtained from the NFG and ED techniques are also given in figure 11 and table 9. The fairly good conformity between the results of the DE and NFG is evident. Additionally the EUL technique partly supports the results of the DE optimization. Thus, it can be mentioned here that the depth of the iron deposit is most likely shallower than the one obtained from previous study by Oruç (2013).

4.2. Deep-seated structure, Sea of Marmara, northwest Turkey

The second field example includes an airborne TMA of a deep-seated magnetized body in the Sea of Marmara, northwest Turkey. The 1600 km long North Anatolian Fault (NAF) extends from eastern Anatolia to the Sea of Marmara in a zone along north Anatolia. The NAF reached the Sea of Marmara as a major fault in the Late Pliocene (Ateş et al 2009). The Sea of Marmara and its surroundings have been affected by three main splay branches of the NAF zone since the Middle Miocene (Okay et al 1991, Aldanmaz et al 2000). Thus, in addition to its complex geology, the study area is located in a neo-tectonically active region. Total field magnetic surveys of Turkey were performed by MTA in

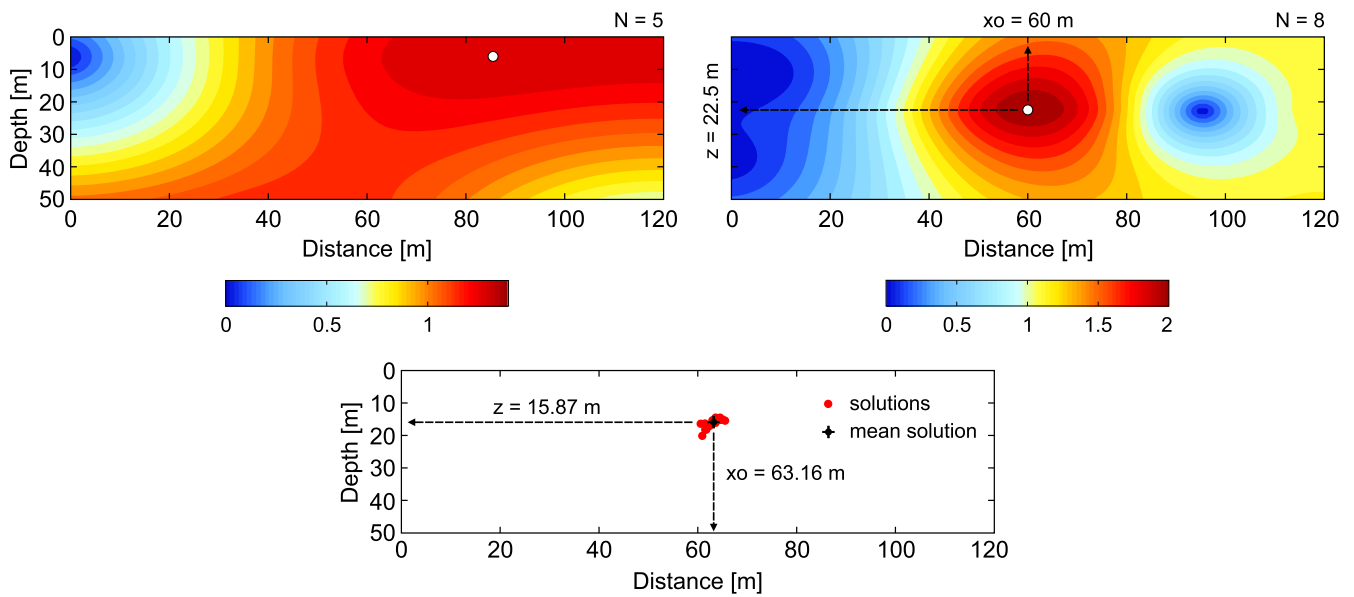


Figure 11. The NFG sections (upper panels) and EUL solutions (lower panel) of the TMA observed over the Kesikkörü iron deposit. Note that the optimum value of N was found to be 8 for the NFG computation.

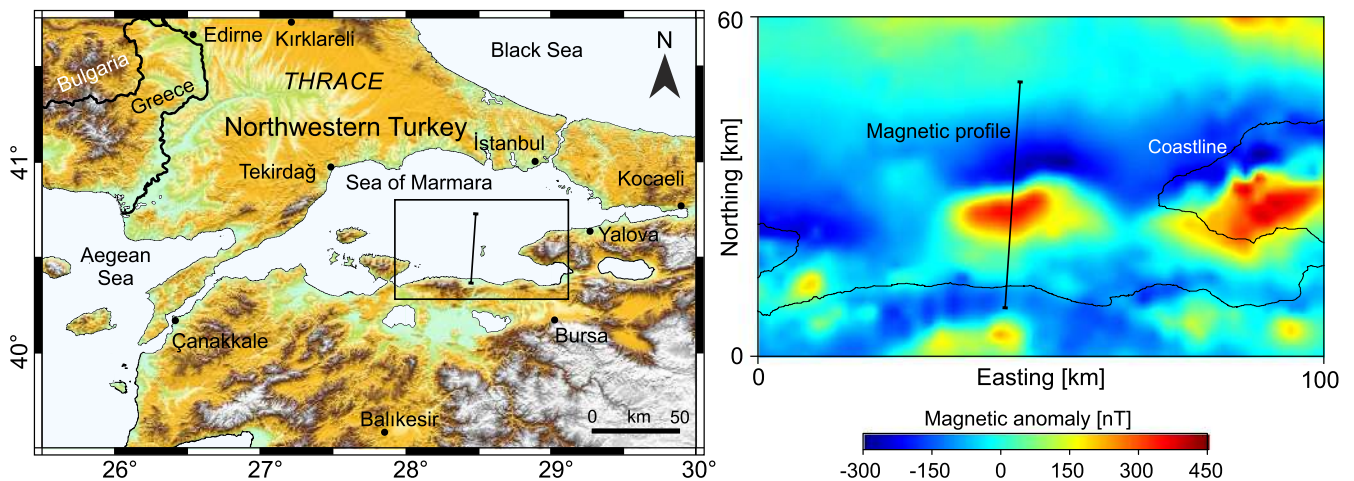


Figure 12. The left panel shows the location map including the studied profile, right panel shows the airborne TMA of the region and the studied profile.

the years between 1975 and 1989. The magnetic data were collected with 1–2 km profile intervals. Flight height and record intervals were about 625 m and 70 m, respectively. Measured airborne magnetic data were corrected for diurnal variations and heading errors, and IGRF 1985 correction was also applied to the observed data set by MTA. The TMA map of the entirety of Turkey can be found in some published literature (e.g., Ates *et al* 1999, MTA 2010). The location and TMA map of the study area are shown in figure 12. A regular-shaped magnetic anomaly is conspicuously seen in the anomaly map. It was reported that the fractures of the faults in the study area and its surroundings were filled with magmatic material where the fault movement reaches magma (Tuncer *et al* 1991). Hence this anomaly is most likely caused by this type of magnetized structure. This structure was previously interpreted by Ateş *et al* (2009) using a 35 km long profile with 19 equispaced data points crossing the anomaly zone,

and they reported a non-flat top surface dike body having an average depth of 2 km. In this study, this anomaly was analysed in a more detailed manner. A 40 km long profile with a sampling interval of 1 km was taken over the anomaly zone (figure 12). The TMA is shown in the left panel of figure 13. Search space parameters used in the DE optimization and the best statistical results obtained at the end of the 30 independent runs are given in tables 7 and 8, respectively. The right panel of figure 13 illustrates the fit between the ASAs calculated from TMA and the best-fitting model response. The inversion result indicated an intermediate case between a thin dike and a contact ($q = 0.79$) having a depth of about 3.78 km and an exact origin of 19.97 km over the cross section (table 9). Moreover, depths of about 3.58 km and 3.52 km from the sea level were obtained with the help of NFG and ED techniques, respectively (table 9 and figure 14). All of these solutions clearly revealed a very well agreement

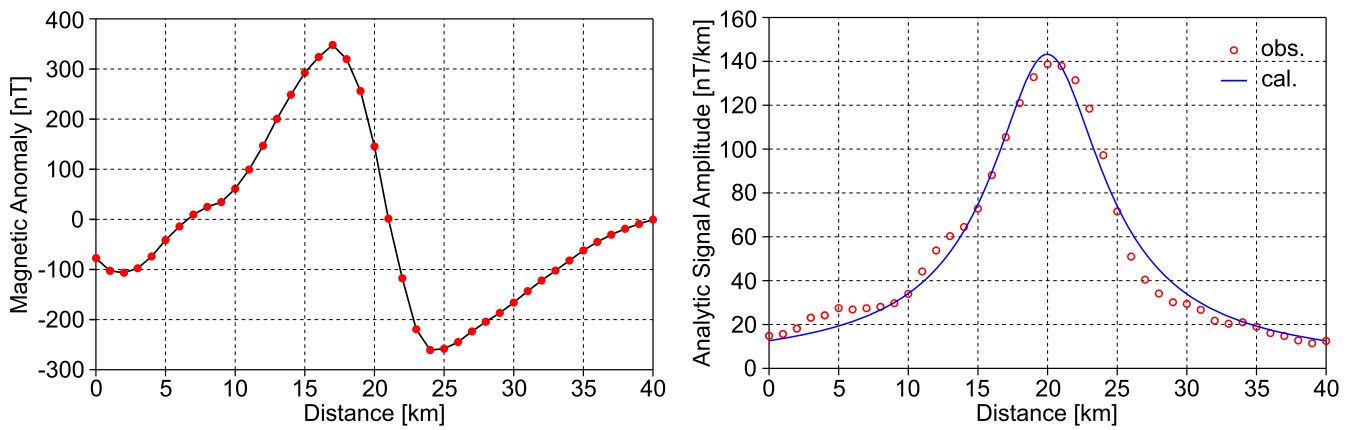


Figure 13. TMA observed over the Sea of Marmara (left panel) and the fit between the ASAs calculated from TMA and the response of best-fitting model parameters estimated via DE algorithm (right panel).

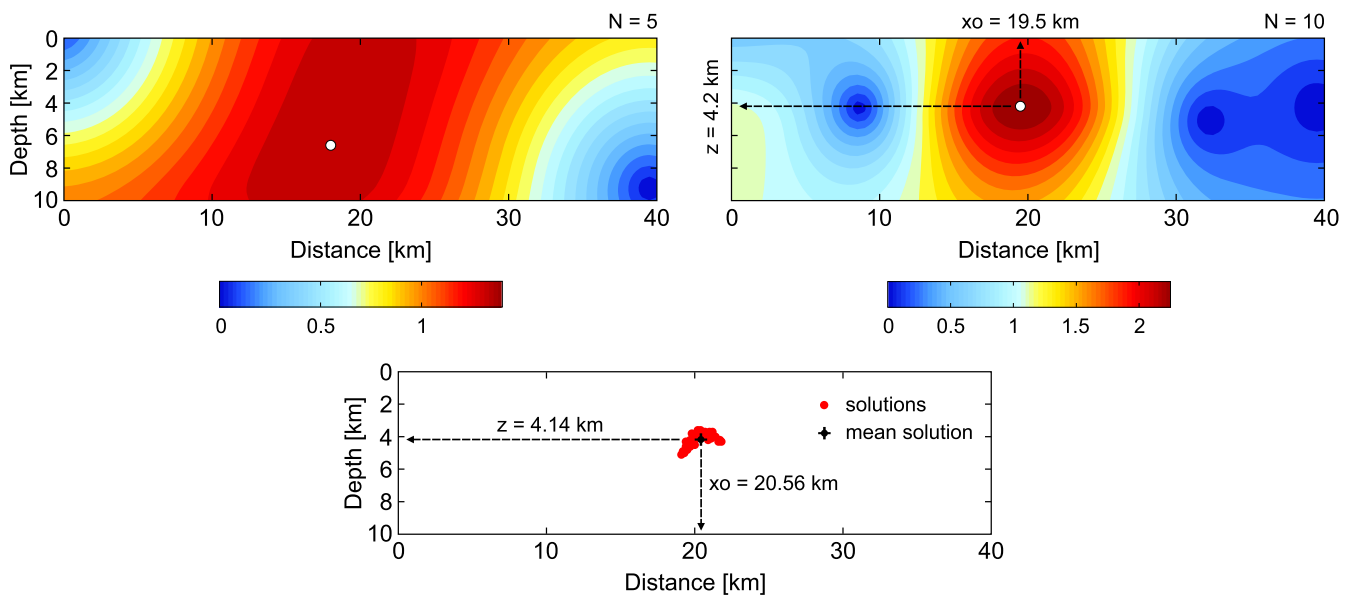


Figure 14. The NFG sections (upper panels) and EUL solutions (lower panel) of the TMA observed over the Sea of Marmara. Note that optimum value of N was found to be 10 for the NFG computation and the flight height was not taken into consideration in the illustrations.

to confirm the accuracy of each interpretation. Thus, this study suggests that the depth of the magnetized structure is deeper than the one suggested by Ateş *et al* (2009).

5. Conclusions

The efficiency and robustness of the DE algorithm, a derivative-free population-based evolutionary metaheuristic, was tested on the inversion of magnetic profile anomalies. Since the ASA computed using the first-order horizontal and vertical derivatives of the observed magnetic anomaly is independent of the ambient field and magnetization directions of the source bodies, the DE optimizations were performed using the ASA computed via frequency domain filtering operations. Before the inversion studies, optimum control parameters in the DE such as crossover probability, mutation scale factor and population size were also determined through some parameter tuning studies to increase the efficacy and the

stability of the metaheuristic for the problem under consideration. Additionally, the produced prediction error energy maps let us better understand the nature of the studied inverse problem. The error image maps clearly indicated that the model parameters i.e. depth, exact origin and shape factor can substantially be estimated by avoiding local optima using the forward modelling equation of the ASA. Synthetic simulations including the magnetic responses of single and multiple source bodies clearly verified the behaviours of error energy maps, even using large search space bounds. Analysing some real data examples using the TMAs of an iron deposit (Kesikköprü-Bala, central Turkey) and a deep-seated magnetized body (Sea of Marmara, northwest Turkey) yielded reasonable solutions. Furthermore, the results obtained by the means of DE optimization were supported by commonly-used and well-established data processing techniques in magnetic anomaly interpretation such as NFG and EUL. The studied causative magnetized bodies have not been studied and reported in the published literature more than once to date.

The implications obtained in this study clearly give new insights into the nature of these causative geological structures. Hence the findings of this work are thought to lead to the future investigations dealing with these anomalies. Applications also indicated that DE/*best/1/bin*, an elitist strategy, used in the DE algorithm exhibits satisfactory behaviours in terms of resolvability, stability and convergence speed of solutions. Consequently, this study revealed that the DE algorithm with stochastic search strategies is a useful tool in both spatial (depth and exact origin) and physical (source geometry) parameters estimation problems based on the ASA of magnetic anomalies without introducing a well-constructed initial model.


Acknowledgments

Thanks are due to Dr Bülent Oruç for providing the TMA of the Kesikköprü iron deposit. We also owe special thanks to two anonymous referees and an editorial board member for their detailed and constructive criticisms which helped us to substantially improve the early version of the manuscript. The location map in figure 12 was generated using Generic Mapping Tools (GMT) (Wessel and Smith 1995). Scilab, the free software for numerical computation (<http://scilab.org/>), which is a trademark of INRIA (<http://inria.fr/>) was used to implement the DE code. Scilab version of DE algorithm written by Walter Di Carlo and Helmut Jarausch is publicly available online at <http://icsi.berkeley.edu/~storn/code.html>.

ORCID iDs

Yunus Levent Ekinci  <https://orcid.org/0000-0003-4966-1208>

Çağlayan Balkaya  <https://orcid.org/0000-0002-0191-8564>

Gökhan Göktürkler  <https://orcid.org/0000-0002-2842-0766>

References

- Agarwal B N P and Srivastava S 2008 FORTRAN codes to implement enhanced local wave number technique to determine location, depth and shape of the causative source using magnetic anomaly *Comput. Geosci.* **34** 1843–9
- Aldanmaz E, Pearce J A, Thirlwall M F and Mitchell J G 2000 Petrogenetic evolution of late Cenozoic, post-collision volcanism in western Anatolia, Turkey *J. Volcanol. Geoth. Res.* **102** 67–95
- Ateş A, Büyüksaraç A, Bilim F, Bektaş Ö, Şendur Ç and Komanovalı G 2009 Spatial correlation of the aeromagnetic anomalies and seismogenic faults in the Marmara region, NW Turkey *Tectonophysics* **478** 135–42
- Ates A, Kearey P and Tufan S 1999 New gravity and magnetic anomaly maps of Turkey *Geophys. J. Int.* **136** 499–502
- Aydın A 2007 Interpretation of gravity anomalies with the normalized full gradient (NFG) method and an example *Pure Appl. Geophys.* **164** 2329–44
- Balkaya Ç 2013 An implementation of differential evolution algorithm for inversion of geoelectrical data *J. Appl. Geophys.* **98** 160–75
- Balkaya Ç, Ekinci Y L, Göktürkler G and Turan S 2017 3D non-linear inversion of magnetic anomalies caused by prismatic bodies using differential evolution algorithm *J. Appl. Geophys.* **136** 372–86
- Balkaya Ç, Göktürkler G, Erhan Z and Ekinci Y L 2012 Exploration for a cave by magnetic and electrical resistivity surveys Ayvacık sinkhole example Bozdağ İzmir (western Turkey) *Geophysics* **77** B135–46
- Başokur A T, Akça I and Siyam N W A 2007 Hybrid genetic algorithms in view of the evolution theories with application for the electrical sounding method *Geophys. Prospect.* **55** 393–406
- Bektaş Ö, Büyüksaraç A and Rozimant K 2013 3D modelling and structural investigation of the central volcanics in Slovakia using magnetic data *Carpath. J. Earth Environ. Sci.* **8** 27–33
- Berezkin V M 1967 Application of the total vertical gradient of gravity for determination of the depths to the sources of gravity anomalies *Explor. Geophys.* **18** 69–79
- Berezkin V M 1973 *Using in Oil-Gas Exploration of Gravity Method* (Moscow: Nedra)
- Berezkin V M 1988 *The Full Gradient Method in Geophysics* (Moscow: Nedra)
- Bhattacharyya B K 1980 A generalized multibody model for inversion of magnetic anomalies *Geophysics* **45** 255–70
- Bingöl E 1989 Geological map of Turkey scale 1/2.000.000 (MTA (General Directorate of Mineral Research and Exploration of Turkey) Publications)
- Biswas A 2016 Interpretation of gravity and magnetic anomaly over thin sheet-type structure using very fast simulated annealing global optimization technique *Model. Earth Syst. Environ.* **2** 30
- Biswas A and Sharma S P 2014 Optimization of self-potential interpretation of 2D inclined sheet-type structures based on very fast simulated annealing and analysis of ambiguity *J. Appl. Geophys.* **105** 235–47
- Biswas A and Sharma S P 2015 Interpretation of self-potential anomaly over idealized body and analysis of ambiguity using very fast simulated annealing global optimization *Near Surf. Geophys.* **13** 179–95
- Boschetti F, Dentith M C and List R D 1996 Inversion of seismic refraction data using genetic algorithms *Geophysics* **61** 1715–27
- Boztuğ D 1998 Post-collisional central Anatolian alkaline plutonism Turkey *Turkish J. Earth Sci.* **7** 145–65
- Chen J, Chouteau M and Keating P 2009 Joint inversion of magnetic anomaly due to kimberlite pipe and its analytic signal *11th SAGA Biennial Technical Meeting & Exhibition* (Swaziland) pp 222–6
- Cheyney S, Fishwick S, Hill I A and Linford N T 2015 Successful adaptation of three-dimensional inversion methodologies for archaeological-scale total-field magnetic data sets *Geophys. J. Int.* **202** 1271–88
- Dannemiller N and Li Y 2006 A new method for determination of magnetization direction *Geophysics* **71** L69–73
- Dewangan P, Ramprasad T, Ramana M V, Desa M and Shailaja B 2007 Automatic interpretation of magnetic data using Euler deconvolution with nonlinear background *Pure Appl. Geophys.* **164** 2359–72
- Di Maio R, Rani P, Piegari E and Milano L 2016 Self-potential data inversion through a genetic-price algorithm *Comput. Geosci.* **94** 86–95
- Dondurur D 2005 Depth estimates for slingram electromagnetic anomalies from dipping sheet-like bodies by the normalized full gradient method *Pure Appl. Geophys.* **162** 2179–95
- Doo W, Hsu S and Yeh Y 2007 A derivative-based interpretation approach to estimating source parameters of simple 2D magnetic sources from Euler deconvolution the analytic-signal method and analytical expressions of the anomalies *Geophys. Prospect.* **55** 255–64
- Doğan B, Ünü T and Sayılı İ S 1998 An approach to the origin of Kesikköprü (Bala-Ankara) iron deposit *Bull. Min. Res. Exp.* **120** 1–35

- Durrheim R J and Cooper G R J 1998 EULDEP: a Fortran program for the Euler deconvolution of magnetic and gravity data *Comput. Geosci.* **24** 545–50
- Ekinci Y L 2016 MATLAB-based algorithm to estimate depths of isolated thin dike-line sources using higher-order horizontal derivatives of magnetic anomalies *SpringerPlus* **5** 1384
- Ekinci Y L, Balkaya Ç, Göktürkler G and Turan S 2016 Model parameter estimations from residual gravity anomalies due to simple-shaped sources using differential evolution algorithm *J. Appl. Geophys.* **129** 133–47
- Ekinci Y L, Balkaya Ç, Şeren A, Kaya M A and Lightfoot C S 2014 Geomagnetic and geoelectrical prospecting for buried archaeological remains on the upper city of Amorium, a Byzantine city in midwestern Anatolia Turkey *J. Geophys. Eng.* **11** 015012
- Ekinci Y L and Yiğitbaş E 2012 A geophysical approach to the igneous rocks in the Biga Peninsula (NW Turkey) based on airborne magnetic anomalies: geological implications *Geodin. Acta* **25** 267–85
- Ekinci Y L and Yiğitbaş E 2015 Interpretation of gravity anomalies to delineate some structural features of Biga and Gelibolu peninsulas and their surroundings (north-west Turkey) *Geodin. Acta* **27** 300–19
- Fedi M and Rapolla A 1999 3D Inversion of gravity and magnetic data with depth resolution *Geophysics* **64** 452–60
- Fernández-Martínez J L, García-Gonzalo E, Fernández Álvarez J P, Kuzma H A and Menéndez Pérez C O 2010 PSO: a powerful algorithm to solve geophysical inverse problems application to a 1D-DC resistivity case *J. Appl. Geophys.* **71** 13–25
- Fregoso E and Gallardo L A 2009 Cross-gradients joint 3D inversion with applications to gravity and magnetic data *Geophysics* **74** L31–42
- Gerovska D and Arauzo-Bravo M J 2003 Automatic interpretation of magnetic data based on Euler deconvolution with unprescribed structural index *Comput. Geosci.* **29** 949–60
- Göksu H, Kaya M A and Kökçe A 2005 Solution of inverse electromagnetic problem of spontaneous potential (SP) by very fast simulated reannealing (VFSR) *Lect. Notes Comp. Sci.* **3611** 622–5
- Göktürkler G 2011 A hybrid approach for tomographic inversion of crosshole seismic first-arrival times *J. Geophys. Eng.* **8** 99–108
- Göktürkler G and Balkaya Ç 2012 Inversion of self-potential anomalies caused by simple geometry bodies using global optimization algorithms *J. Geophys. Eng.* **9** 498–507
- Jung K 1961 *Schwerkraftverfahren in der angewandten Geophysik Akademische Verlagsgesellschaft Gees und Portig KG Leipzig* 94–5
- Keating P and Sailhac P 2004 Use of the analytic signal to identify magnetic anomalies due to kimberlite pipes *Geophysics* **69** 180–90
- Kuşcu İ and Erler A 1998 Mineralization events in a collision-related setting: the Central Anatolian Crystalline Complex, Turkey *Int Geol Rev* **40** 532–65
- Lelievre P G and Oldenburg D W 2009 A 3D total magnetization inversion applicable when significant complicated remanence is present *Geophysics* **74** L21–30
- Li X and Yin M 2012 Application of differential evolution algorithm on self-potential data *PLoS One* **7** 1–11
- Li Y and Oldenburg D W 1996 3D inversion of magnetic data *Geophysics* **61** 394–408
- Li Y and Oldenburg D W 2003 Fast inversion of large-scale magnetic data using wavelet transforms and a logarithmic barrier method *Geophys. J. Int.* **152** 251–65
- Liu S, Hu X, Liu T, Xi Y, Cai J and Zhang H 2015 Ant colony optimisation inversion of surface and borehole magnetic data under lithological constraints *J. Appl. Geophys.* **112** 115–28
- Monteiro Santos F A 2010 Inversion of self-potential of idealized bodies' anomalies using particle swarm optimization *Comput. Geosci.* **36** 1185–90
- Morris B, Ugalde H and Thomson V 2007 Magnetic remanence constraints on magnetic inversion models *The Lead. Edge* **26** 960–4
- MTA (General Directorate of Mineral Research and Exploration of Turkey) 2010 Airborne regional aeromagnetic anomaly map of Turkey (MTA Publications) scale: 1/2000000
- Nabighian M N 1972 The analytic signal of two-dimensional magnetic bodies with polygonal cross-section: its properties and use for automated anomaly interpretation *Geophysics* **37** 507–17
- Okay A I, Siyako M and Bürkan K A 1991 Geology and tectonic evolution of the Biga Peninsula, northwest Turkey *Bull. Tech. Uni. Istanbul* **44** 191–255
- Oruç B 2013 Determination of horizontal locations and depths of magnetic sources using continuous wavelet transform *Yerbilimleri* **34** 177–90
- Oruç B and Keskinsezer A 2008 Detection of causative bodies by normalized full gradient of aeromagnetic anomalies from east Marmara region, NW Turkey *J. Appl. Geophys.* **65** 39–49
- Pallero J L G, Fernandez-Martinez J L, Bonvalot S and Fudym O 2015 Gravity inversion and uncertainty assessment of basement relief via particle swarm optimization *J. Appl. Geophys.* **116** 180–91
- Parasnis D S 1986 *Principles of Applied Geophysics* 4th edn (New York: Chapman and Hill)
- Pekşen E, Yas T, Kayman A Y and Özkan C 2011 Application of particle swarm optimization on self-potential data *J. Appl. Geophys.* **75** 305–18
- Pekşen E, Yas T and Kıyak A 2014 1D DC resistivity modeling and interpretation in anisotropic media using particle swarm optimization *Pure Appl. Geophys.* **171** 2371–89
- Peñuñuri F, Cab C, Carvente O, Zambrano-Arjona M A and Tapia J A 2016 A study of the classical differential evolution control parameters *Swarm Evol. Comput.* **26** 86–96
- Portniaguine O and Zhdanov M S 2002 3D magnetic inversion with data compression and image focusing *Geophysics* **67** 1532–41
- Price K V, Storn R M and Lampinen J A 2005 *Differential Evolution: A Practical Approach to Global Optimization* (Berlin: Springer)
- Qing A 2009 *Differential Evolution: Fundamentals and Applications in Electrical Engineering* (New York: Wiley)
- Rabeh T and Khalil A 2015 Characterization of fault structures in southern Sinai Peninsula and Gulf of Suez region using geophysical data *Environ. Earth Sci.* **73** 1925–37
- Rao D B and Babu N R 1991 A rapid method for three-dimensional modeling of magnetic anomalies *Geophysics* **56** 1729–37
- Reid A B, Allsop J M, Granser H, Millet A J and Somerton I W 1990 Magnetic interpretation in three dimensions using Euler deconvolution *Geophysics* **55** 80–91
- Rikitake T, Sato R and Hagiwara Y 1976 *Applied Mathematics for Earth Scientists* (Tokyo: Terra Scientific)
- Roest W and Pilkington M 1993 Identifying remanent magnetization effects in magnetic data *Geophysics* **58** 653–9
- Roy A 1962 Ambiguity in geophysical interpretation *Geophysics* **27** 90–9
- Salem A 2005 Interpretation of magnetic data using analytic signal derivatives *Geophys. Prospect.* **53** 75–82
- Salem A, Ravat D, Mushayandebvu M F and Ushijima K 2004 Linearized least-squares method for interpretation of potential-field data from sources of simple geometry *Geophysics* **69** 783–8
- Shamsipour P, Chouteau M and Marcotte D 2011 3D stochastic inversion of magnetic data *J. Appl. Geophys.* **73** 336–47
- Sharma S P and Biswas A 2011 Global nonlinear optimization for the estimation of static shift and interpretation of 1D magnetotelluric sounding data *Ann. Geophys.* **54** 249–64
- Shaw R and Srivastava S 2007 Particle swarm optimization: a new tool to invert geophysical data *Geophysics* **72** F75–83

- Shearer S and Li Y 2004 3D inversion of magnetic total gradient data in the presence of remanent magnetization *Proc. of the 74th Annual Int. Meeting, SEG* pp 774–7
- Sheng Z and Xiaohong M 2015 Improved normalized full-gradient method and its application to the location of source body *J. Appl. Geophys.* **113** 86–91
- Singh A and Biswas A 2016 Application of global particle swarm optimization for inversion of residual gravity anomalies over geological bodies with idealized geometries *Nat. Resour. Research* **25** 297–314
- Song X, Li L, Zhang X, Shi X, Huang J, Cai J, Jin S and Ding J 2014 An implementation of differential search algorithm (DSA) for inversion of surface wave data *J. Appl. Geophys.* **111** 334–45
- Srivastava S and Agarwal B N P 2010 Inversion of the amplitude of the two-dimensional analytic signal of magnetic anomaly by the particle swarm optimization technique *Geophys. J. Int.* **182** 652–62
- Srivastava S, Datta D, Agarwal B N P and Mehta S 2014 Applications of ant colony optimization in determination of source parameters from total gradient of potential fields *Near Surf. Geophys.* **12** 373–89
- Stavrev P Y 1997 Euler deconvolution using differential similarity transformations of gravity or magnetic anomalies *Geophys. Prospect.* **45** 207–46
- Storn R 2008 *Differential Evolution Research—Trends and Open Questions* Advances in Differential Evolution, SCI 143 ed U K Chakraborty (Berlin: Springer-Verlag) pp 1–31
- Storn R and Price K V 1995 *Differential Evolution—A Simple and Efficient Adaptive Scheme for Global Optimization Over Continuous Spaces* Technical Report TR-95-012 (Berkeley, CA: International Computer Science Institute)
- Sındırgı P, Pamukçu O and Özyalın Ş 2008 Application of normalized full gradient method to self potential (SP) data *Pure Appl. Geophys.* **165** 409–27
- Telford W M, Geldart L P, Sheriff R E and Keys D A 1990 *Applied Geophysics* (Cambridge: Cambridge University Press)
- Thompson D T 1982 EULDPH: a new technique for making computer assisted depth estimates from magnetic data *Geophysics* **47** 31–7
- Thurston J B and Smith R S 1997 Automatic conversion of magnetic data to depth, dip, and susceptibility contrast using the SPITM method *Geophysics* **62** 807–13
- Tronicke J, Paasche H and Böniger U 2012 Crosshole traveltime tomography using particle swarm optimization: a near-surface field example *Geophysics* **77** R19–32
- Tuncer M K, Oshiman N, Baris S, Kamaci Z, Kaya M A, Isikara A M and Honkura Y 1991 Further evidence for anomalous magnetic structure along the active fault in western Turkey *J. Geomag. Geoelectr.* **43** 937–50
- Wessel P and Smith W H F 1995 New version of the generic mapping tools *EOS Trans. Am. Geophys. Union* **76** 329
- Yang X S 2014 *Nature-Inspired Metaheuristic Algorithms* (London: Elsevier)
- Yu Z, Zhaosheng N and Shige J 2014 An improved differential evolution algorithm for nonlinear inversion of earthquake dislocation *Geodesy Geodynamic* **5** 49–56
- Zeng H, Meng X, Yao C, Li X, Lou H, Guang Z and Li Z 2002 Detection of reservoirs from normalized full gradient of gravity anomalies and its application to Shengli oil field, east China *Geophysics* **67** 1138–47
- Zhou T-F, Peng G-X, Hu T-Y, Duan W-S, Yao F-C and Liu Y-M 2014 Rayleigh wave nonlinear inversion based on the Firefly algorithm *Appl. Geophys.* **11** 167–78
- Zunino A, Benvenuto F, Armadillo E, Bertero M and Bozzo E 2009 Iterative deconvolution and semiblind deconvolution methods in magnetic archaeological prospecting *Geophysics* **74** L43–51